Rare Metal Materials and Engineering
Volume 51, Issue 9, September 2022
Available online at www.rmme.ac.cn

Science Press

Cite this article as: Wang Junfeng, Xia Min, Wu Jialun, et al. Ladle Nozzle Clogging in Vacuum Induction Melting Gas Atomization: Influence of Delivery-Tube Geometry[J]. Rare Metal Materials and Engineering, 2022, 51(09): 3214-3222.

ARTICLE

Ladle Nozzle Clogging in Vacuum Induction Melting Gas Atomization: Influence of Delivery-Tube Geometry

Wang Junfeng, Xia Min, Wu Jialun, Ge Changchun

Institute of Special Ceramics and Powder Metallurgy, University of Science and Technology Beijing, Beijing 100083, China

Abstract: The nozzle clogging in vacuum induced melting gas atomization (VIGA) process was investigated. To understand the influence of tip shape of the delivery-tube on nozzle clogging more accurately, the interface tracking method of computational simulation fluid volume was adopted to simulate the two-phase flow in the primary atomization region. Results show that the small platform at the end of the draft tube is the key factor leading to the nozzle clogging. Therefore, the expansion angle (30°, 35°, 40°, 45°) of the delivery-tube is improved to shorten the width of the small platform. Thus, the nozzle clogging is solved, the atomization continuity is realized, and the atomization efficiency is improved. Additionally, when the expansion angle is 40°~45°, the powder has better morphology with the particle size of 21~25 μm. The numerical simulation results under different modification aspects display similar trends to the experiment ones. This research is of guidance significance and reference value to understand the nozzle clogging process of VIGA process.

Key words: alloy; powder; gas atomization; delivery-tube; nozzle clogging

Metal powders have been widely applied in the field of additive manufacturing (AM) due to their good particle size distribution[1-3], sphericity[4], and powder morphology[5,6], which significantly affects the mechanical properties and microstructure of the industrial products[7]. Currently, the fine spherical metal powders for AM are mainly produced by the vacuum induction melting gas atomization (VIGA) technique, which has fine process controllability and high production efficiency[8,9]. During VIGA, the metal is molten in a vacuum induction furnace, then passes through the tundish, and finally flows out from the delivery-tube. The metal flow is atomized into spherical powders by interactions with the supersonic gas[10-13]. However, in the industrial production, the nozzle clogging seriously restricts the atomization continuity. The metal flow accumulates at the edge of the close-coupled nozzle, resulting in the temperature decrease of the metal flow and then leading to the blocked nozzle and the atomization termination.

In VIGA production, the nozzle clogging is unpredictable and complex. The metal flow interacts with the supersonic gas and spreads radially at the upper end of the stagnation point in the recirculation zone. Then, the flow end gradually becomes thinner and forms unstable wave-like structures, which eventually break up into ligaments and large droplets. When the atomization parameters change, the primary atomization becomes disordered and the nozzle clogging appears. In the long-term industrial production, it is found that the tip geometry of the delivery-tube has significant influence on the nozzle clogging. Miller et al[14] studied the influence of delivery-tube on the gas in recirculation zone in order to improve the coupling degree between the gas and the melt. Due to the complexity of the atomization gas-flow field, CFD software is usually used to simulate the delivery-tube geometry design[15,16]. Anderson et al[17] demonstrated that the internal structure of the delivery-tube affects the fragmentation law of the melt in the primary atomization area. Moreover, Unal et al[18] reduced the consumption of atomized gas and increased the economic benefit by optimizing the delivery-tube geometry. However, few studies investigate the influence of delivery-tube geometry on the nozzle clogging.

In this research, the nozzle clogging during VIGA was investigated by analyzing the end expansion angle of the

Received date: September 10, 2021
Foundation item: Central University Basic Research Fund of China (FRF-GF-19-0058)
Corresponding author: Xia Min, Ph. D., Associate Professor, Institute of Special Ceramics and Powder Metallurgy, University of Science and Technology Beijing, Beijing 100083, P. R. China, E-mail: xmdsg@ustb.edu.cn.

delivery-tube. The Euler-Euler method, volume of fluid (VOF) analysis, multiphase flow model, and the large eddy simulation (LES) model[10] were adopted to simulate the primary atomization in the recirculation zone. Thus, the influence of the alloy melt on nozzle clogging and the formation mechanism were discussed. With the fixed alloy melt temperature, viscosity, and atomization gas pressure, four expansion angles were selected to observe the movement pattern of alloy melt in the delivery-tube during the primary atomization process. The numerical simulation results and experiment ones were compared. The expansion angle of the modified delivery-tube was 30°, 35°, 40°, and 45°. The Ni-based superalloy was used as the raw material. The atomized powders were characterized by the fine powder yield, particle size distribution, and powder morphology. The mechanism of nozzle clogging in industrial VIGA process was studied.

1 Experiment

The schematic diagram of VIGA setup is shown in Fig. 1a. The high frequency induction furnace was used to melt the Ni-based alloy in vacuum atmosphere. The molten alloy flowed into the atomization chamber along the delivery-tube (Fig. 2) and was atomized by supersonic gas, as shown in Fig. 1c. The close-coupled annular nozzle was applied. The load capacity of the alumina crucible was 40 kg, the maximum heating temperature of the induction furnace was 2050 K, the vacuum degree of the equipment was 3.0×10^{-4} Pa, and the power was 70 kW. The heating rate of the alloy ingot was 50 K/min in the early stage and 80~100 K/min in the later stage. The temperature of the atomized Ni-based alloy melt was 1880 K. The gas flow meter (LZB-15) was installed on the gas pipeline to measure the gas flow rate. The measuring range was 1~20 m^3/h. The atomization of the alloy melt near the delivery-tube was observed by the high-speed camera. After the powder preparation, it was cooled for 2 h in the powder collecting tank to prevent oxidation. Finally, the particle size distribution of the powder was detected, and the surface morphology of the Ni-based superalloy powder was observed by the scanning electron microscope (SEM).

The delivery-tube plays a connecting role between the alloy ingot melting stage and gas atomization stage. In order to shorten the width of the small platform at the delivery-tube tip and to reduce the contact area with alloy droplets, based on the traditional draft tube structure (Fig. 2a) and the delivery-tube geometry[19,20], four delivery-tubes with expansion angles of 30°, 35°, 40°, and 45° were used in this research and denoted as Type 1, Type 2, Type 3, and Type 4, respectively, as shown in Fig. 2b. The delivery-tube length was 13 cm and the inner diameter was 4 mm. The protruding length of the delivery-tube was 3 mm.

The width of atomizer nozzle is 0.5 mm. The composition of the Ni-based alloy is shown in Table 1. The atomization pressure was 3.5 MPa. The melt mass flow rate was estimated according to the ratio of melt mass to total atomization duration. The gas mass flow rate was measured. The ratio of melt mass flow rate to gas mass flow rate, namely GMR, is an important parameter for VIGA process. The experiment parameters are shown in Table 2.

2 Numerical Model Simulation

2.1 Boundary conditions and mesh

The geometric model for the numerical simulation of the close-coupled annular nozzle is the 2D axisymmetric swirl, which can simplify the simulation calculation and obtain the accurate gas-flow field results, compared with the 3D model.

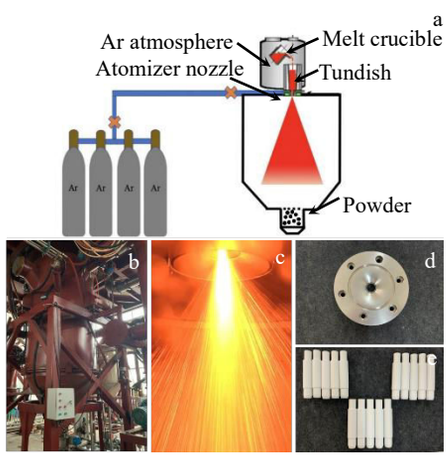

Fig.1 Schematic diagram (a) and appearance (b) of VIGA setup; appearance of alloy flow in VIGA process (c); appearances of close-coupled annular nozzle (d) and delivery-tube (e)

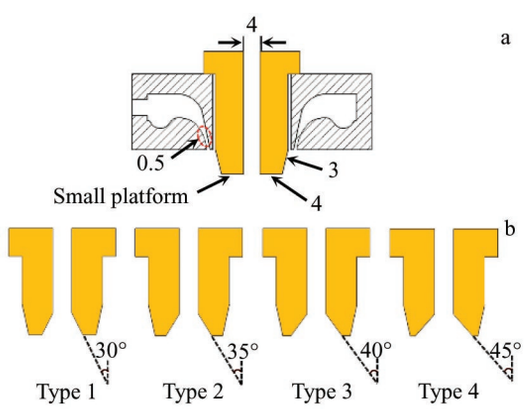

Fig.2 Schematic diagram of close-coupled annular nozzle and delivery-tube (a); schematic diagrams of delivery-tubes with different tip angles (b)

Table 1 Composition of Ni-based alloy (wt%)

Ni	Co	Cr	W	Ti	Al	Mo	Ta	Nb	C	B	Zr
45.70~46.20	20.00~22.00	12.00~14.00	4.10~4.50	3.30~3.70	3.30~3.70	2.50~2.90	1.40~1.80	1.30~1.70	0.02~0.04	0.02~0.03	0.04~0.07

Table 2 Experiment parameters of VIGA processes with different expansion angles

Parameter	Type 1	Type 2	Type 3	Type 4
Expansion angle/(°)	30	35	40	45
Delivery-tube inner diameter/mm	4	4	4	4
Nozzle slit width/mm	0.5	0.5	0.5	0.5
Gas temperature/K	273	273	273	273
Atomization pressure/MPa	3.5	3.5	3.5	3.5
Melt mass flow rate/kg·h^{-1}	560.70	494.12	400.25	365.22
Gas mass flow rate/kg·h^{-1}	620	620	620	620
GMR	1.1	1.2	1.5	1.7
Melt superheat/K	150	150	150	150

As the melt flow falls freely through the delivery-tube into the atomization chamber, the melt flow boundary into the atomization chamber is set as the velocity inlet boundary. The gas enters the atomization chamber through the pressure inlet. The physical parameters of melt and atomization gas are shown in Table 3[9]. The simulated boundary conditions of the primary atomization region near the nozzle (60 mm×155 mm) include the following parameters: pressure inlet (atomization gas inlet), velocity inlet (alloy melt flow inlet), pressure outlet, and no-slip wall. Table 4 shows the initial boundary conditions for the simulation. The detailed numerical simulation methods are shown in Table 5.

Fig. 3b shows the unencrypted mesh in the simulation domain by GAMBIT software. The mesh size near the nozzle and the pressure outlet area is 0.1 and 0.4 mm, respectively. Besides, the total number of grids is 162 800. The internal boundary mesh is compatible between the adjacent parts of the model, thereby initiating the converging calculation. In order to obtain the detailed analysis of the metal flow breaking process, the dynamic mesh adaptive method was applied to encrypt the grid, as shown in Fig.3c. The minimum grid size is 0.025 mm and the total number of grids is 470 000. The simulation shows that the droplets can be accurately presented, and the visualization quality of the melt atomization process is improved. In order to verify that the grid number of mesh has no effect on the gas flow velocity, the velocity changes of AB and CD lines (marked in Fig.3a) are shown in Fig.4 and Fig.5, respectively. It is found that the gas velocity at the nozzle outlet and along the axis (recirculation zone) barely changes with varying the grid number of meshes, which further proves that the mesh is independent.

2.2 Primary atomization breakup model

VOF model was used to simulate the two-phase flow inside the delivery-tube and near the nozzle exit. Since the atomized gas at the nozzle exit is supersonic, the k-ε model was used to simulate the high-speed internal flow, which accurately predicts the related shock wave. The supersonic gas is compressible during the atomization. This simulation mainly describes the interactions between the metal flow and gas, the formation of droplets, and the exchange of energy[21]. Only the physical changes were modelled in this research. Hence, the continuity equation and momentum equation[22] are expressed by Eq.(1) and Eq.(2), respectively, as follows:

$$\frac{\partial}{\partial t}(\alpha\rho) + \nabla\cdot(\alpha\rho\boldsymbol{\mu}) = 0 \tag{1}$$

$$\frac{\partial}{\partial t}(\rho\boldsymbol{u}) + \nabla\cdot(\rho\boldsymbol{u}\boldsymbol{u}) = -\nabla P + \nabla\cdot[\mu(\nabla\boldsymbol{u} + \nabla\boldsymbol{u}^T)] + \rho\boldsymbol{g} + \boldsymbol{F} \tag{2}$$

where u, P, ρ, μ, α, and F are the velocity, pressure, density, viscosity, surface tension, and the indicator fields, respectively; T is the material temperature; t is the time; $\boldsymbol{g}$ is the gravitational acceleration. Eq. (1) and Eq. (2) include the pressure gradient term, the gravitational body forces, the viscous stresses, and the capillary forces induced by surface tension. The surface tension and energy[23] can be described, as follows:

$$\frac{\partial\alpha}{\partial t} + \nabla\cdot\alpha u = 0 \tag{3}$$

$$\frac{\partial}{\partial t}(\rho E) + \nabla\cdot[\boldsymbol{u}(\rho E + P)] = \nabla\cdot(k_{\text{eff}}\nabla T) + S_{\text{T}} \tag{4}$$

where E is the internal energy of material, S_{T} is the viscous dissipation term, and k_{eff} is the effective thermal conductivity. k_{eff} can be calculated from the average of the two-phase volumetric fraction.

LES model was adopted to visualize the fine droplets of atomized metal flow, because it can filter out turbulence and divide the turbulence into large and small eddies. Yoshizawa[24] and Menon[25] et al proposed a sub-grid kinetic energy model, and the transport equation for this model is as follows:

Table 3 Physical parameters of Ni-based alloy and argon gas[9]

Parameter	Density/kg·m^{-3}	Heat capacity/J·kg^{-1}·K^{-1}	Thermal conductivity/ W·m^{-1}·K^{-1}	Molecular mass/ kg·mol^{-1}	Viscosity/kg·m^{-1}·s^{-1}
Ni-based alloy	7055.84	720	29.6	48	0.05
Argon gas	1.784	520.65	0.016	39.95	2.125×10^{-5}

Table 4 Initial boundary conditions for simulation

Parameter	Value
Pressure inlet/MPa	3.5
Pressure outlet/MPa	0
Velocity inlet/m·s^{-1}	2
Ni-based alloy temperature/K	2000
Argon gas temperature/K	300
Ni-based alloy content/vol%	100
Argon gas content/vol%	0

$$\frac{\partial(\bar{\rho}\overline{k}^{sgs})}{\partial t}+\frac{\partial(\overline{\rho u_j}\overline{k}^{sgs})}{\partial x_j}=-\tau_{ij}^{sgs}\frac{\partial\overline{u}_j}{\partial x_j}+\varepsilon^{sgs}-\frac{\partial}{\partial x_j}\left(\frac{v_t\partial k^{sgs}}{\sigma_k\partial x_j}\right) \quad (5)$$

where k^{sgs} is the sub-grid kinetic energy, τ^{sgs} is the sub-grid stress, v_t is the sub-grid viscosity coefficient, ε^{sgs} is the turbulent energy dissipation rate, u_j is the velocity, σ_k is a constant, x is coordinate, i and j represent directions, and the overline indicates the average value of corresponding parameter.

Table 5 Numerical simulation methods

Method	Single-phase simulation	Multi-phase simulation
Geometry	2D axisymmetric swirl	2D axisymmetric swirl
Computing time	Unsteady time step of 10^{-7} s	Unsteady time step of 10^{-8} s
Flow model	Single-phase (atomization gas)	Multi-phase-VOF (gas and alloy)
Turbulence model	K-epsilon	K-epsilon and LES

3 Results and Discussion

3.1 Nozzle clogging

Fig. 6 shows the process of nozzle clogging in VIGA process. The alloy melt at the nozzle outlet blocks the delivery-tube with unreasonable design. According to Fig. 6b and 6c, it is found that the temperature of the alloy melt remaining in the melting chamber is reduced, and eventually the melt remains in the intermediate frequency furnace and tundish. Once the nozzle clogging occurs in actual VIGA production, the tundish, delivery-tube, and nozzle need to be replaced instantly, which reduces the production efficiency and decreases the economic benefit. The nozzle clogging happens really fast, resulting in the difficulty in observation of the clogging process during atomization. Therefore, the numerical simulation was used to analyze the nozzle clogging.

3.2 Nozzle clogging mechanism

The FLUENT software was used to simulate the movement direction of the alloy melt during the primary atomization for the analysis of the formation mechanism of the nozzle clogging, as shown in Fig.7.

The schematic diagram of the structure of gas-flow field below the melt delivery-tube is shown in Fig. 7a. When the

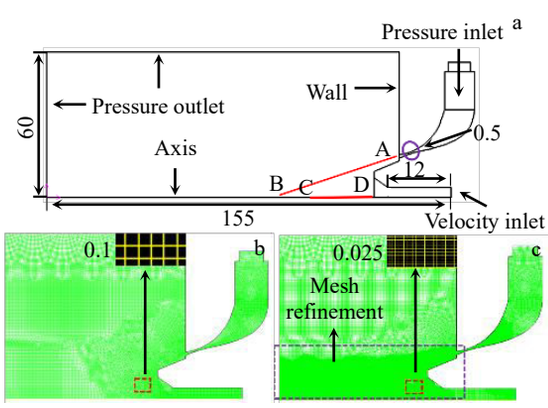

Fig.3 Simulation computational domain and boundary conditions (a); unencrypted (a) and encrypted (b) meshes in primary atomization domain

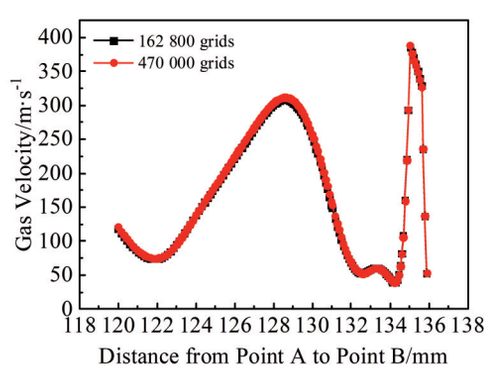

Fig.4 Influence of grid number of mesh on gas velocity along AB line marked in Fig.3a

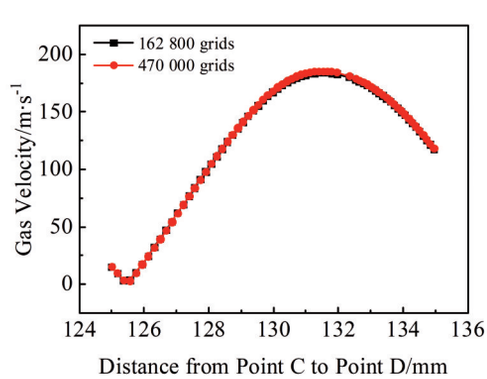

Fig.5 Influence of grid number of mesh on gas velocity along CD line marked in Fig.3a

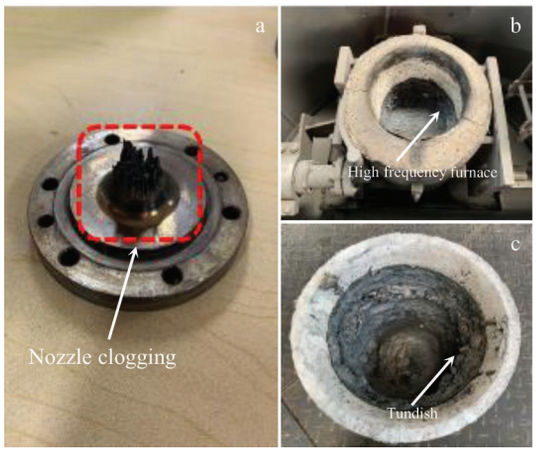

Fig.6 Appearances of nozzle clogging in VIGA production at delivery-tube tip (a), intermediate frequency furnace (b), and tundish (c)

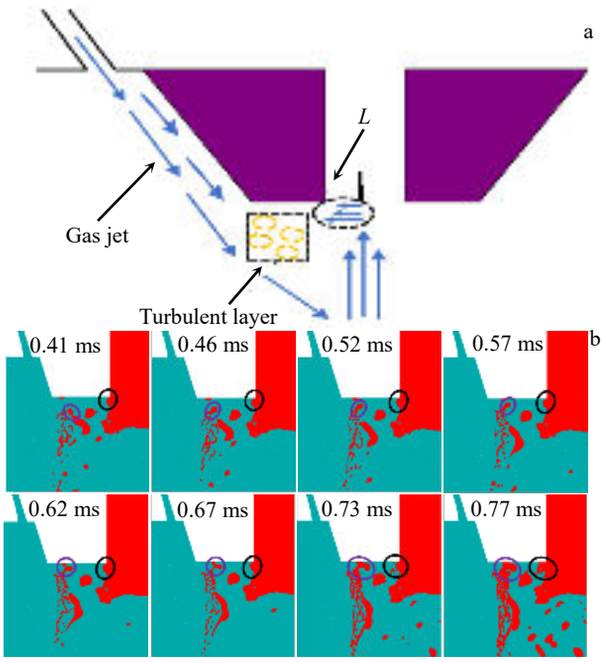

Fig.7 Formation mechanisms of nozzle clogging during alloy melt atomization: (a) gas-flow direction in recirculation zone; (b) evolution of alloy melt in primary atomization process (*L*: distance from the axis of recirculation zone to small platform of delivery-tube)

upward flow in the recirculation zone encounters the downward alloy melt, the melt movement direction deflects along the radial direction. There are many turbulent vortices distributed on the sonic boundary of the recirculation zone, which forms the turbulent layer[26]. In the turbulent region, the momentum exchange occurs between the alloy melt and the gas, which accelerates the primary atomization process of the alloy melt. Fig. 7b shows the evolution of alloy melt near the delivery-tube at different atomization time. The black circles in Fig. 7b indicate the surface of alloy liquid column. The alloy melt gradually accumulates on the inner edge of the delivery-tube due to the upward gas-flow.

After the alloy melt leaves the delivery-tube, the surface of the melt liquid film under the "umbrella structure"[25] is disturbed by the atomization gas, and the Rayleigh-Plateau instability occurs[26]. Due to the surface tension, the ligament collapses under the effect of gas intensity, forming many irregular spheres (droplets) and liquid lines, which are marked by purple circles in Fig. 7b. In the turbulent region, partial alloy droplets move downward for secondary atomization and further break into smaller droplets. Other alloy droplets remain on the small platform at the delivery-tube tip. It can be found that the nozzle clogging process starts on both sides of the small platform of the delivery-tube and moves towards the center. Therefore, reducing the width of the small platform at the delivery-tube tip and increasing the distance between the alloy melt and the inner edge of delivery-tube in the recirculation zone are both beneficial to avoid the nozzle clogging.

Fig. 8a and 8b present the simulated and experiment results of conventional nozzle without delivery-tube with expansion angle during the primary atomization process. When the melt encounters the atomization gas in the recirculation zone, it spreads along the radial direction. The alloy melt gradually accumulates on the small platform of the delivery-tube. In the low-temperature gas environment, the cooling speed of the melt flow is very fast. After the atomization proceeds for 1.1 ms, the alloy melt gradually adheres to the delivery-tube tip. This phenomenon appears in both the experiment and simulated processes. However, as shown in Fig. 8c, the metal flow is divided along the radial directions in the recirculation zone, and the edge gradually becomes thinner. The alloy melt begins to interact with the atomized gas before it touches the inner wall of the delivery-tube. Then the melt breaks into droplets and liquid lines. Because the melt edge is close to the supersonic free boundary, the crushing effect is more intense. The metal flow cannot stay near the nozzle when it moves along the supersonic flow direction, resulting in the

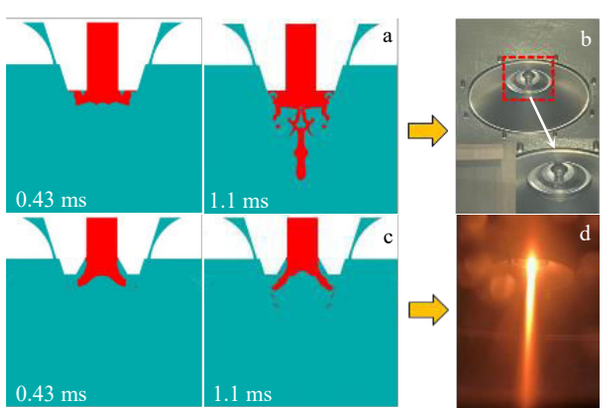

Fig.8 Simulation (a, c) and experiment (b, d) results of nozzles without (a, b) and with (c, d) delivery-tube with expansion angle of 35° in primary atomization process

continuous atomization.

3.3 Influence of expansion angle of delivery-tube on nozzle clogging

The axial velocity cloud diagrams of the delivery-tubes with different expansion angles are shown in Fig. 9. With increasing the expansion angle, the width of the small platform at the delivery-tube tip is decreased, the area of the recirculation zone is increased in the gas-flow field, and the position moves up, therefore significantly reducing the blockage probability of alloy melt and improving the atomization efficiency. The velocity distributions at the inner edge of the delivery-tubes are marked by red circles in Fig.9. When the expansion angle is increased from 30° (Fig. 9a) to 35° (Fig. 9b), the velocity distribution area is small, which is mainly distributed at the included angle between the delivery-tube outlet and the small platform. However, when the expansion angle is increased from 40° (Fig. 9c) to 45° (Fig.9d), the velocity distribution area is enlarged, and there is gas turbulence in the inner wall of the delivery-tube, which can reduce the adhesion probability between the alloy melt and the delivery-tube exit.

Fig. 10 shows the axial velocity of the gas-flow field of nozzles with different expansion angles. It can be found that the core velocity of the recirculation zone is the closest to the velocity of the delivery-tube tip when the expansion angle is 30° . Besides, with increasing the expansion angle, the core velocity position of the recirculation zone remains. As shown in Fig. 9, the white dotted lines (L_1~L_4) indicate the distance from the axis of the recirculation zone to the small platform of the delivery-tube. It can be observed that the distance is increased from 3.5 mm to 5.5 mm gradually with increasing the expansion angle from 30° to 45°. When the intensity of the recirculation zone is basically the same, with increasing the distance, the alloy melt moves downward along the radial direction with the gas flow in the turbulent zone without connection with the small platform.

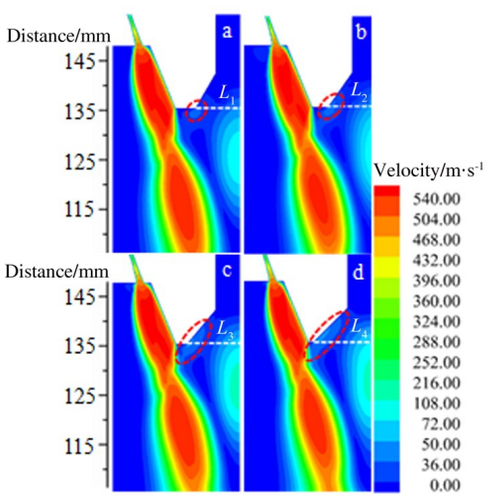

Fig.9 Velocities of nozzles with delivery-tubes with expansion angle of 30° (a), 35° (b), 40° (c), and 45° (d)

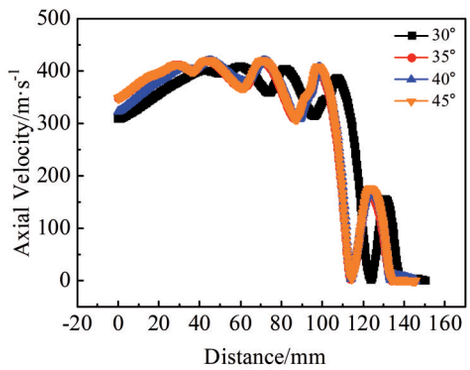

Fig.10 Axial velocities along the center of the computational domain for delivery-tubes with different expansion angles

The turbulent area of the flow field is between the supersonic gas flow and the recirculation zone, with many inside vortices. The atomization process is transient, and the large turbulent kinetic energy indicates that the interaction between gas and melt is strong[27]. According to Fig. 11, when the expansion angle is 30°, the small platform at the delivery-tube tip is wide. Due to the uncertainty of the turbulence vortex direction, the probability of droplet collision is increased and the droplets stick to the small platform more easily after primary atomization. However, with increasing the expansion angle, the turbulent kinetic energy marked by the red rectangles in Fig.11 is gradually decreased, resulting in the decrease of the non-directional motion intensity of the melt droplets in the turbulent region. Besides, the secondary atomization occurs with the downward movement of the air flow.

Fig.12 shows the primary atomization cloud diagrams of Ni-based alloy melt with delivery-tubes with different expansion angles. The alloy melt presents the “umbrella structure”[25] due to the upward gas flow in the recirculation zone and spreads along the radial directions. Due to the Rayleigh-Plateau

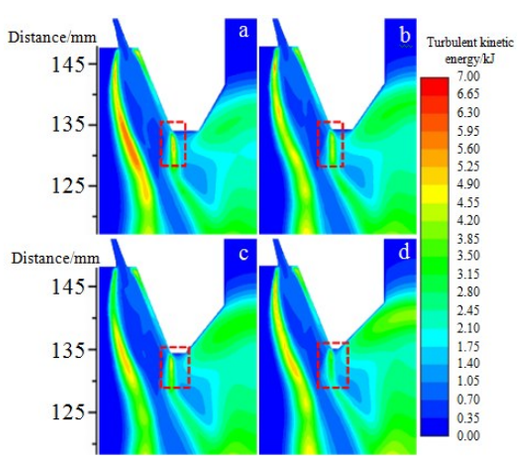

Fig.11 Turbulent kinetic energy cloud diagrams near the small platform of delivery-tubes with expansion angle of 30° (a), 35° (b), 40° (c), and 45° (d)

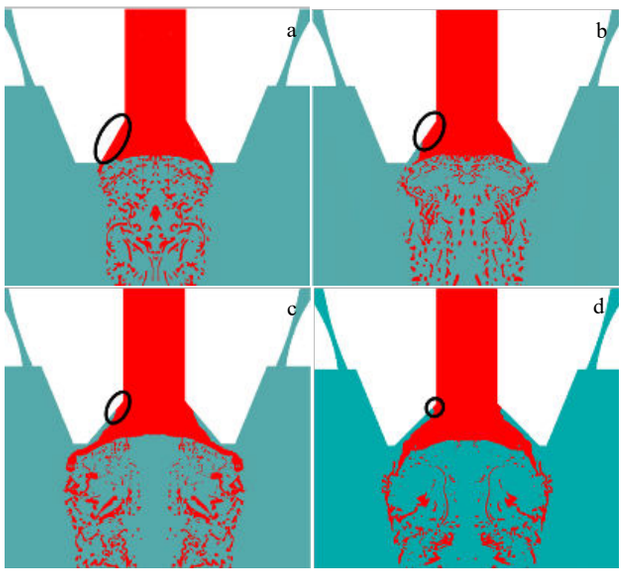

Fig.12 Primary atomization processes of Ni-based melt with delivery-tubes with expansion angle of 30° (a), 35° (b), 40° (c), and 45° (d)

instability[26] effect, the melt liquid film decomposes into many ligaments and large droplets by surface tension. By optimizing the geometry of the delivery-tube tip, the melt droplets do not adhere to the outer wall and small platform during the atomization process. The alloy melt is in contact with the inner wall of the delivery-tube, as shown in the black circles in Fig. 12. With increasing the expansion angle, the contact area is shrunk, which reduces the risk of cracking at the delivery-tube tip and increases the service life of delivery-tube. As shown in Fig.12c and 12d, it can be observed that the alloy droplets and liquid lines after primary atomization are closer to the supersonic free boundary, which increases the intensity of interaction with the gas, resulting in the improvement of the final fine powder yield.

The atomization moment of alloy droplets is difficult to capture, due to the high melt temperature and short atomization crushing duration. In order to better observe the structure of recirculation zone and the distribution of melt droplets in the atomization process, the water was used instead of alloy melt flow. Fig. 13a shows the appearance of flow field without the delivery-tube at pressure of 2 MPa. With the annular nozzle, the converging point is concentrated obviously, and a stable recirculation zone is formed at the delivery-tube tip, which can atomize and break the alloy melt. From Fig. 13b, with increasing the expansion angle of the delivery-tube, the distribution angle of small water droplets after atomization is increased, and the finer the particle size, the blurrier the atomization edge. This result is consistent with the simulation results in Fig. 12, indicating the prediction accuracy.

The times of continuous atomization of one delivery-tube are an important index to evaluate the stability of atomizer. According to Table 6, the times of continuous atomization with delivery-tubes with expansion angle of 30° and 35° are less than those of 40° and 45° due to the large contact area between the alloy melt and the inner wall of the delivery-tube. Besides, the longer the atomization duration of each atomization process, the more the alloy melts adhering to the inner wall, which eventually leads to the crack of wall. In the actual production, the occurrence of wall crack indicates the update of new delivery-tube. When the expansion angle is 45°, the inner wall of the delivery-tube is hardly in contact with the alloy melt, thus greatly increasing the service life of delivery-tube.

3.4 Powder size

As shown in Fig. 14, most powders are spherical with smooth surface. It can be observed that when the expansion angle is 30° and 35°, the powder particle size is large, and the irregular spherical and rod powders appear, accompanied by many satellite powders. With increasing the expansion angle, the powder particle size becomes smaller, the powder

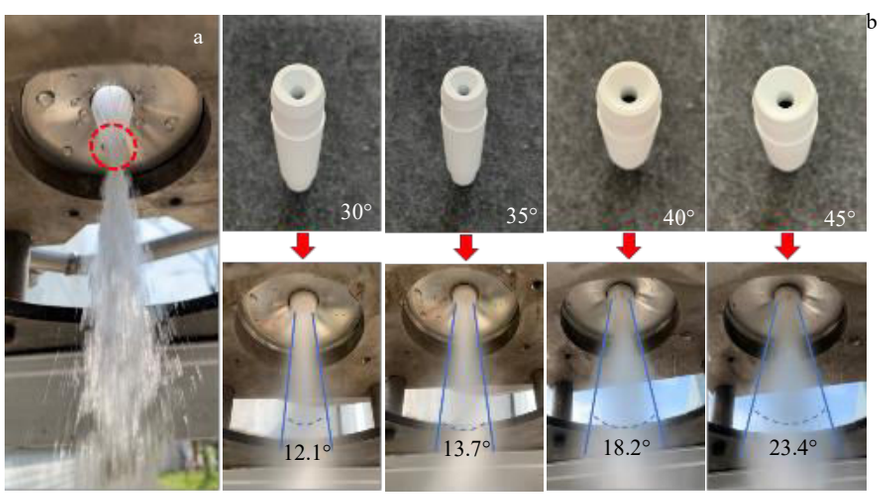

Fig.13 Appearances of flow field without delivery-tube at pressure of 2 MPa (a) and atomization processes with delivery-tubes with different expansion angles at pressure of 3.5 MPa

Table 6 Atomization time and durations of each furnace with delivery-tubes with different expansion angles

Expansion angle/(°)	Continuous atomization duration/s									
	1st	2nd	3rd	4th	5th	6th	7th	8th	9th	10th
30	54	62	81	-	-	-	-	-	-	-
35	52	55	61	69	87	-	-	-	-	-
40	56	54	57	61	63	65	68	84	-	-
45	51	53	54	53	55	54	57	56	62	65

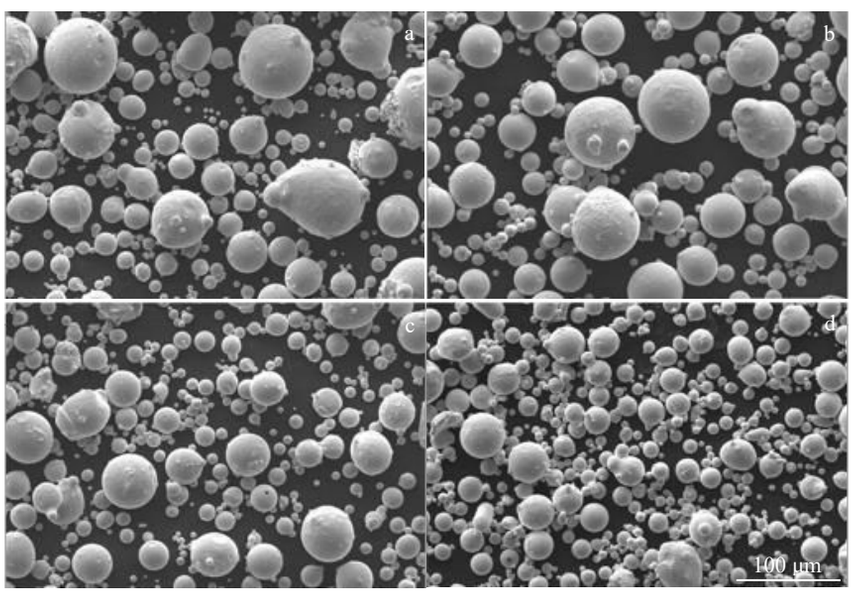

Fig.14 SEM morphologies of powders prepared by delivery-tubes with expansion angle of 30° (a), 35° (b), 40° (c), and 45° (d)

sphericity is improved, and the amount of satellite powder is decreased. Due to the high surface tension, rapid cooling rate, and large momentum of powders with small particle sizes, the collisions occur between the not-completely-solidified large droplets, forming the satellite powder. Therefore, the powders generated by the delivery-tube with large expansion angles are more spherical and smoother than those with small angles, and the formation of satellite powder is also less.

The particle size distribution was measured under the delivery-tubes with different expansion angles, as shown in Fig.15. The powder particle size is decreased with increasing the expansion angle of the delivery-tube. When the expansion angle is 30° and 35°, the powder particle size is about 44 μm; when the expansion angle is 40° and 45°, the practical size is 21~25 μm. In conclusion, the application of larger expansion angle of delivery-tube can decrease the particle size. In addition, according to the industrial application, the amount of used argon, power consumption, and economic cost can be reduced by 20% after the improvement of the delivery-tube.

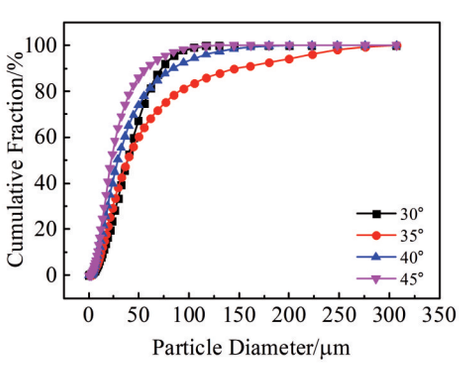

Fig.15 Particle size distributions of powders prepared by delivery-tubes with different expansion angles

4 Conclusions

1) When the expansion angle of delivery-tube is 40°~45°, the primary atomized Ni-based alloy melt breaks into many droplets and liquid lines of different sizes, which is conducive to the secondary atomization. The particle size of powder prepared by delivery-tube with large expansion angle is 21~25 μm, and the satellite powder and irregularly powder are less.

2) The optimization of the geometry of delivery-tube can improve the vacuum induction melting gas atomization (VIGA) production and improve the economic benefit by improving the atomization efficiency. The influence of other factors, such as viscosity and inclusions, on the nozzle clogging should be further studied to achieve better atomization continuity in VIGA process.

References

1 Kaiser R, Li C G, Yang S S *et al*. *Advanced Powder Technology* [J], 2018, 29(3): 623

2 Yang L B, Ren X N, Xia M *et al*. *Rare Metal Materials and Engineering*[J], 2020, 49(6): 2017

3 Motaman S, Mullis A M, Cochrane R F *et al*. *Metallurgical and Materials Transactions B*[J], 2015, 46(4): 1990

4 Wei M W, Chen S Y, Sun M *et al*. *Powder Technology*[J], 2020, 367: 724

5 Wei M W, Chen S Y, Sun M *et al*. *Aircraft Engineering and Aerospace Technology*[J], 2002, 74(5): 181

6 Singh D, Dangwal S. *Journal of Materials Science*[J], 2006, 41(12): 3853

7 Feng S, Xia M, Ge C C. *International Journal of Material Forming*[J], 2019, 12(4): 615

8 Metz R, Machado C, Houabes M *et al*. *Journal of Materials Processing Technology*[J], 2007, 195(1-3): 248

9 Xia Min, Wang Peng, Zhang Xiaohu *et al*. *Acta Physica Sinica* [J], 2018, 67(17): 41 (in Chinese)

10 Mates S P, Settles G S. *Atomization and Spray*[J], 2005, 15(1): 41

11 Anderson I E, Terpstra R L. *Materials Science and Engineering A* [J], 2002, 326(1): 101

12 Ting J, Anderson I E. *Materials Science and Engineering A*[J], 2004, 379(1-2): 264

13 Firmansyah D A, Kaiser R, Zahaf R. *Japanese Journal of Applied Physics*[J], 2014, 53(5S3): 05HA09

14 Miller S A. *United States Patent*, 4619597[P], 1986

15 Zeoli N, Gu S. *Computational Materials Science*[J], 2008, 42(2): 245

16 Mi J, Figliola R S, Anderson I E. *Metallurgical and Materials Transactions B*[J], 1997, 28(5): 935

17 Anderson I E, Terpstra R L, Figliola R S. *Advances in Powder Metallurgy and Particulate Materials*[J], 2004, 2: 26

18 Unal R. *Powder Metallurgy*[J], 2007, 50(4): 302

19 Zhao Xinmin, Xu Jun, Zhu Xuexin *et al*. *The Chinese Journal of Nonferrous Metals*[J], 2009, 19(5): 967 (in Chinese)

20 Mullis A M, McCarthy I N, Cochrane R F. *Journal of Materials Processing Technology*[J], 2011. 211(9): 1471

21 Liu Xinling, Chen Xing, Hou Xueqin *et al*. *Rare Metal Materials and Engineering*[J], 2009, 38(7): 1179 (in Chinese)

22 Song Xinqiang, Li Yuxi, Han Meng. *Powder Metallurgy Industry* [J], 2018, 28(1): 68 (in Chinese)

23 Zhong Z Y, Saka H, Kim T H *et al*. *Materials Science Forum*[J], 2005, 475-479: 37

24 Yoshizawa A, Horiuti K A. *Journal of the Physical Society of Japan*[J], 1985, 54(8): 2834

25 Menon S, Yeung P K, Kim W W. *Computers and Fluids*[J], 1996, 25(2): 165

26 Zeoli N, Gu S. *Computational Materials Science*[J], 2006, 38(2): 282

27 Kaltz T, Glogowski M, Micci M M. *30th AIAA, ASME, SAE, and ASEE Joint Propulsion Conference and Exhibit*[C]. Indianapolis: AIAA, 1994

真空感应熔炼气体雾化过程中钢包喷嘴堵塞:导流管几何形状的影响

王军峰，夏　敏，吴嘉伦，葛昌纯

(北京科技大学 粉末冶金与先进陶瓷研究所，北京 100083)

摘　要：研究了真空感应熔炼气体雾化（VIGA）技术中喷嘴堵塞的过程。为了更准确地了解导流管顶端形状对喷嘴堵塞的影响，采用计算模拟流体体积界面跟踪方法，对一次雾化区的两相流进行了模拟。结果表明，导流管末端的小平台是导致喷嘴堵塞的关键因素。因此，改进了输送管的扩张角（30°、35°、40°、45°），缩短了小平台的宽度，解决了喷嘴堵塞的问题，实现了雾化连续性，提高了雾化效率。此外，当扩张角为40°~45°时，粉末具有较好的微观形貌，粒径为21~25 μm。不同改进角度下的数值模拟结果与实验结果显示出相似的趋势。本研究对了解VIGA工艺喷嘴堵塞过程具有指导意义和参考价值。

关键词：合金；粉末；气雾化；导流管；堵漏包

作者简介：王军峰，男，1990年生，博士生，北京科技大学粉末冶金与先进陶瓷研究所，北京 100083，E-mail：m13840317451@163.com